공학석사 학위논문

# Effect of charge blocking layer

# for enhancing detectivity

# in near infrared organic photodetectors

근적외선 유기광검출기의 검출도 향상을 위한

전하 차단 층의 효과

**2019 년 2 월**

서울대학교 대학원

재료공학부

이 은 지

# Effect of charge blocking layer
# for enhancing detectivity
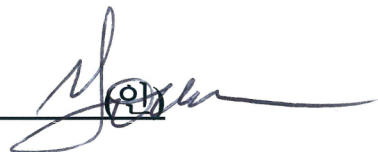# in near-infrared organic photodetectors
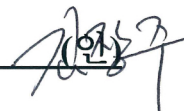
지도 교수 김 장 주

이 논문을 공학석사 학위논문으로 제출함
2019 년 2 월

서울대학교 대학원
재료공학부 재료공학 전공
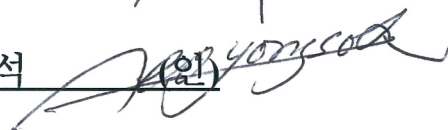이 은 지

이은지의 공학석사 학위논문을 인준함
2019 년 2 월

위 원 장 _____ 윤 재 륜 _____ (인)

부위원장 _____ 김 장 주 _____ (인)

위   원 _____ 서 용 석 _____ (인)

# Abstract

# Effect of charge blocking layer

# for enhancing detectivity

# in near infrared organic photodetectors

Eun-Ji Lee

Department of Materials Science and Engineering

The Graduate School

Seoul National University

Potential of organic semiconductors was proved as the development of organic light emitting diodes (OLEDs) used in many areas of our life. Interest in organic photodetectors is also increasing thanks to an advantage of organic materials such as low process cost, using flexible substrate, wavelength selectivity by designing a molecular structure. Organic photodetectors (OPDs) can be applied in various fields

depending on the absorption wavelength region. Near-infrared photodetectors have the various application of NIR camera, organ implant, motion detector, and remote controller. However, NIR OPDs have a drawback in terms of small bandgap causing high dark current density, namely noise in OPDs. Noise stand out particularly in the photoconductive mode of photodetectors in which an external voltage is applied. An increase in the dark current reduces the detectivity and it is important to improve the detectivity without decreasing the efficiency.

For enhancing the detectivity of OPDs it is required to reduce dark current density and increase external quantum efficiency. The dark current density is originated from the injected carrier from the electrode and thermally generated carrier in the PN junction and leakage current in devices. Reducing the dark current by blocking this flow of charge is important to improve the detectivity.

In this study, we introduced organic materials as charge blocking layers (CBLs) on inverted-structure NIR OPDs to investigate the origin of the dark current density. Depending on CBLs with various molecular energy levels, characteristics of OPDs is different. The deeper HOMO of the charge blocking layer is, the lower the dark current density is. With inserting 4,4'-bis(N-carbazolyl)-1,1'-biphenyl (CBP) between anode and donor the dark current density was reduced up to 164 nA/cm$^2$ and EQE also increased from 25.1% to 29.3%. High detectivity of $1.06 \times 10^{12}$

cm$^2$ Hz/W at 970 nm under a reverse bias of -3V was obtained. The low dark current density was obtained due to low HOMO and high LUMO level of CBP working as energetic barriers on the injected charge from the electrode and thermally generated charge at PN junction respectively.

Other figure of merits including linear dynamic range, cut off frequency, and response time were compared depending on used CBL. The linear region was also longest in the device with CBP due to the low dark current density. However, using charge blocking layers resulted in increased response time compared with the device without CBL because the charge extraction was delayed due to the increase of device thickness and accumulation at the organic interface. Similarly, the cut-off frequency was reduced compared with the device without CBL but high mobility of CBL compensated loss of frequency response.

In this study, we could know the effect of the charge blocking layer on the characteristics of the organic photodetector and it will be useful for the study of material and development of device structure in the future.

**Keywords:** charge blocking layer, organic photodetector, enhancing detectivity, molecular orbital level, inverted near-infrared photodetector, origin of dark current

**Student Number:** 2017 - 29529

# Contents

# List of Tables

# List of Figures

# Chapter 1. Introduction

## 1.1 Motivation and outline of thesis

### 1.1.1 Motivation

Organic photodetectors (OPDs) have received a lot of attention due to advantages such as using flexible substrate, color selectivity, lightweight.

Especially, near-infrared OPDs have various application to CMOS image sensor,[1,2,3] NIR camera, and artificial organ like retinal implants.[4] However, NIR OPDs has low bandgap for absorbing NIR light and its detectivity is relatively low due to high dark current density compared to UV-vis OPDs. Low bandgap causes increasing dark current density consisting of injected charge from the electrode and thermally generated charge at the interface of donor and acceptor.

Therefore, in many papers, the dark current density and the detectivity measured at zero or low bias e.g. -1V have been reported. Photoconductive mode OPDs have the advantage such as high speed and efficiency but, noise, dark current, is also high due to external bias. But OPDs as image sensor are required to combine with transistors and the photoconductive mode is more preferred for high speed. As mentioned,

NIR OPDs have low detectivity and lowering dark current density is required for high detectivity.

The detectivity of photodetectors will be enhanced if the dark current density decrease and EQE increase. Reducing dark current is important on the detectivity in photoconductive mode OPDs because increasing bias increases not only EQE but also dark current density.

In this thesis, we will introduce charge blocking layer for reducing the dark current density in NIR OPDs. It was founded that not only injection carrier from electrode but also thermally generated carrier at the interface between donor and acceptor contribute to the dark current.

### 1.1.2 Outline of thesis

**In chapter 1**, the brief introduction of the organic photodetector including the general working mechanism and the figure of merits were described. Figure of merits included responsivity, detectivity, linear dynamic range, cut off frequency, and response time. Additionally, reviews on organic photodetectors were listed.

**In chapter 2**, we introduced charge blocking layers to reduce dark current density. High LUMO level of CBL blocked injected electron and low HOMO level also suppressed hole flow. Interestingly, the dark current density decreased as the HOMO level is deeper. The dark current density was reduced to 164nA/cm$^2$ at -3V when CBP was used as the

charge blocking layer. Also, EQE increased due to increased hole transport properties between CBP and HATCN. It resulted in the high detectivity of $1.06 \times 10^{12}$ cm$^2$ Hz/W at 970 nm and -3V

**In chapter 3**, the additional figure of merits were measured and compared to the devices. The linearity of photocurrent to light intensity, frequency response, and response time were measured. The linearity of OPDs was also enhanced with inserting charge blocking layer due to reduced dark current density. But, it affects badly on frequency response and response time. Instead, as higher mobility of the charge blocking layer is, the smaller loss of frequency response is. This study could propose criteria on selecting charge blocking layer in OPDs.

## 1.2 Organic photodetectors

### 1.2.1 Photodetectors

Photodetectors are sensors of light or electromagnetic radiation. Many types of photodetectors are grouped by a mechanism such as photoemission, semiconductor, thermal, photochemical properties. Photodetectors using photodiode have more high electrical conductivity when illuminated. These devices can be used as a CMOS image sensor in a digital camera, night vision imager, and spectroscopy. **Figure 1.1**. shows a) image sensor and b) picture captured with Vis-NIR camera. Organic photodetectors to be described in this study use organic materials as semiconductors.

### 1.2.2 Working principles of organic photodetectors

Organic photodetectors using photodiode convert optical signal to electric signal. Organic photovoltaic device consists of conductive electrodes at both sides and organic active layers between them. When light is illuminated to photo-active organic layer, electrons in the HOMO level are excited by absorbing photon and go to the LUMO level
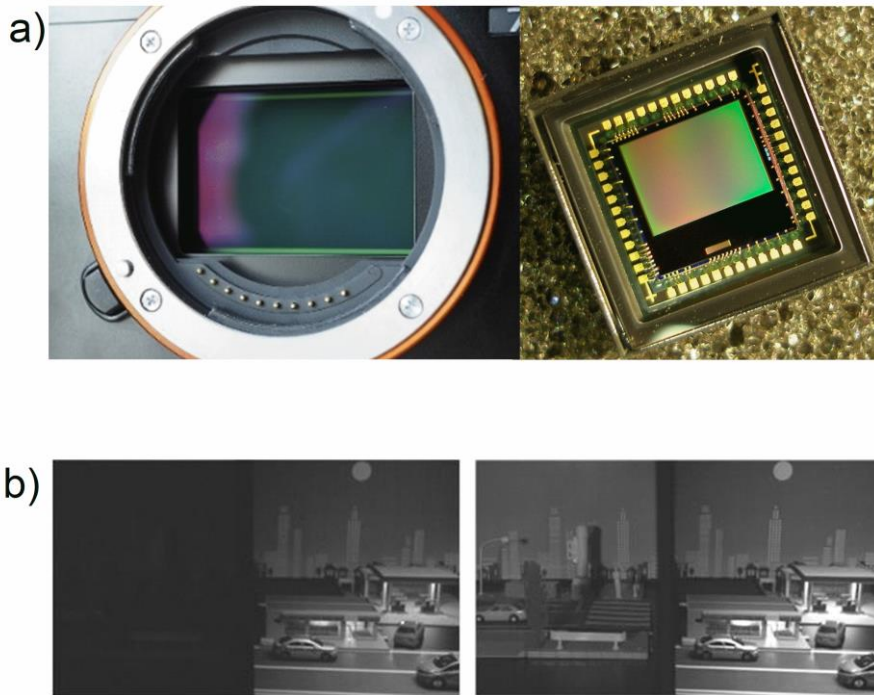
**Figure 1.1** a) CMOS image sensor, according to Coventor Blog by Marketing Wed, June 14, (2017) b) images captured in color imaging mode (Left) and NIR imaging mode (Right), according to Panasonic data February 9, (2017)

remaining holes in the HOMO level. The Electrons and the holes bounded by coulombic interaction are called exciton. To be dissociated, excitons should diffuse to interface between donor and acceptor. Excitons at the interface can be easily dissociated to free carrier electrons and holes. Then, the electrons and the holes drift and diffuse by the internal electric field and collected at the electrode. Schematic mechanism of organic photovoltaic cell is shown in **Figure 1.2**.

There are two working modes of photodetectors, photovoltaic mode and photoconductive mode.

**Photovoltaic mode**

As shown in **Figure 1.2**, photodetectors work on short circuit condition when the voltage is zero in current density-voltage curve. There are drift and diffusion current contributing to short circuit current, so current is obtained without additional bias. Because of no bias, electrical noise is low, but small bandwidth and low speed of the device were exhibited.
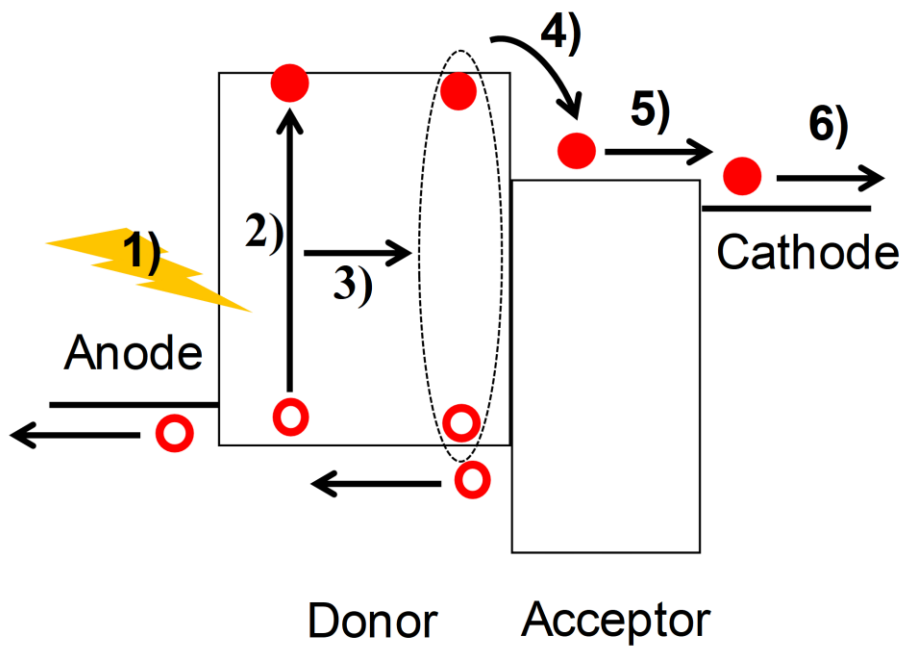
**Figure 1.2** Mechanism of photo-induced carrier generation in photovoltaic cells. 1) Photon absorption, 2) Exciton generation, 3) Exciton diffusion, 4) Exciton dissociation, 5) Carrier transport, 6) Charge collection

**Photoconductive mode**

Differently, a photoconductive mode has an advantage in bandwidth and speed. Owing to external force recombination loss of created carrier are reduced and free carriers are easily collected to the electrode. However, noise is also higher than the photovoltaic mode. In the photodetectors, noise is an important parameter decreasing the detectivity of photodetectors. Although disadvantage, the photoconductive mode is required to operate photodetector for an image sensor which is combined with a n-channel transistor. Therefore, suppressing dark current density is an important issue on research of the photoconductive mode photodetectors.
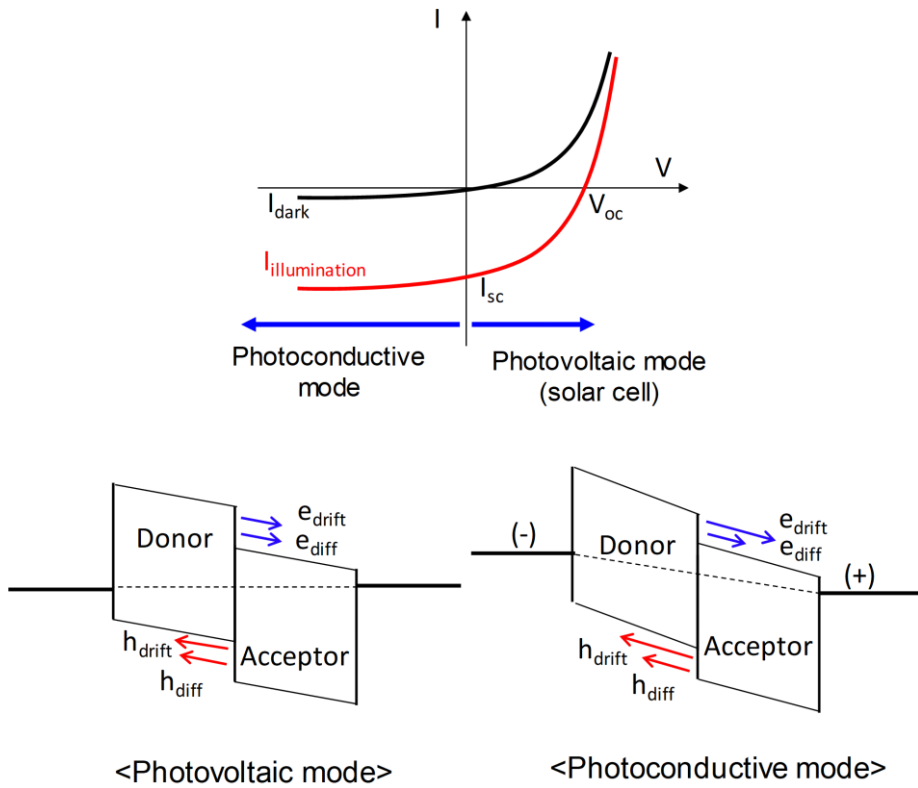
**Figure 1.3** Current-voltage characteristics and schematic energy diagram on working mode of photodetectors

### 1.2.3 Figure of merits of organic photodetectors

Figure of merits of OPDs were introduced to compare and assess the performance of the devices. There are several figure of merits including responsivity, detectivity, linear dynamic range, response time, and cut off frequency.

**External quantum efficiency (EQE) and responsivity (R)**

EQE is ratio of number of incident photon to number to extracted electron.

$$EQE = \frac{I/q}{P/h\nu} = \frac{Rh\nu}{q} \qquad (1.1)$$

I: output photo-induced current

q: elementary charge

P: incident power of photon

$h\nu$: photon energy

EQE can be expressed with responsivity which means ratio of incident light power and output photo-induced current.

$$R = \frac{J_{ph}}{P_{in}} = \frac{EQE \cdot q}{h\nu} \ [A/W] \qquad (1.2)$$

R: responsivity [A/W]

$J_{ph}$: photocurrent density

$P_{in}$: power of incident light

**Noise equivalent power (NEP) and detectivity (D)**

The sensitivity of the device is an ability that detector distinguishes optical input power from noise.

Noise equivalent power is minimum light power which can be detected by the photodetector, power at signal-to-noise ratio (SNR)=1 and bandwidth=1, and power corresponding to the noise current.[5]

$$\text{NEP}= \frac{\text{Input power for SNR=1}}{\sqrt{B}}= \frac{i_{\text{noise}}}{R\sqrt{B}}= \frac{\sqrt{2qi_dB}}{R\sqrt{B}}= \frac{\sqrt{2qi_d}}{R} \ [\text{W}/\sqrt{\text{Hz}}] \qquad (1.3)$$

$$i_{\text{noise}}= \sqrt{i_s^2 + i_{th}^2 + i_{1/f}^2 + i_d^2} \ [\text{A}] \qquad (1.4)$$

$i_s$= shot noise

$i_{th}$= thermal noise (Johnson noise)

$i_{1/f}$= 1/f noise

$i_d$= shot noise from dark current

The dark current is a dominant element to noise of photodetector under operating in photoconductive mode and thermal noise can be negligible. But it cannot directly define noise of photodetectors due to other component contributing to noise so, detectivity can be overestimated.

11

The detectivity (D) is reciprocal of the NEP and specific detectivity (D*) is normalized with respect to the area (A) for comparison with other photodetectors in terms of sensitivity.

$$D^* = \frac{\sqrt{A}}{NEP} = \frac{R\sqrt{A}}{\sqrt{2qi_d}} \quad [cm\sqrt{Hz}/W] \tag{1.4}$$

In order to increase the detectivity, reduction of the dark current and increase of the responsivity are crucial.

**Linear dynamic range (LDR)**

Linear dynamic range means operational light intensity range.[6] The photocurrent is measured depending on intensity of light shown in **Figure 1.4a**

$$LDR = 20\log\left(\frac{I_{max}}{I_{min}}\right) \tag{1.5}$$

This quantifies the ability of the light sensor to adequately detect variation in light intensity. It is expressed as a ratio of maximum and minimum detectable current within a linear region.

So, high LDR is desirable and low dark current density is required because $i_{noise}$ is lower limit of the linear range $I_{min}$.

The deviation in region of high light intensity is related to charge carrier mobility of the active materials and bimolecular recombination rate[7] and photocurrent will deviate from linearity at a certain light intensity (or

photocurrent, $I_{max}$). The deviation in region of low light intensity is related to dark current because the dark current is saturated as light intensity decrease.

**Response time ($t_r$, $t_f$)**

The speed of response in photodetector is the time for charge to generate and extract to the electrode. Rising time and fall time are defined respectively as the time rising from 10% to 90% of photocurrent and falling from 90% to 10% of photocurrent shown in **Figure 1.4b**. It is important parameter for high resolution of image sensor.

**Cut off frequency ($f_{-3dB}$)**

The temporal bandwidth or cut off frequency is defined as the frequency of input light modulation at which the photo-response is -3dB lower than the continuous wave response shown in **Figure 1.4c**. This frequency is limited by the carrier transit time and RC-time. In order to get high response minimizing carrier transit time and decreasing capacitance.
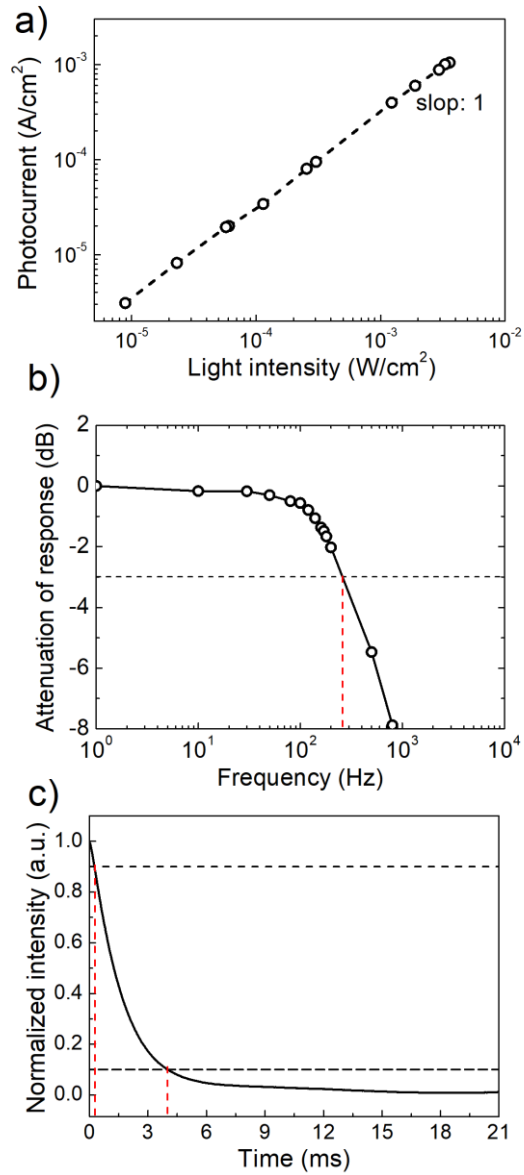
**Figure 1.4** Figure of merits of OPDs such as a) light intensity-photocurrent linearity, b) frequency response (cut off frequency, $f_{-3dB}$), c) response time (fall time)

# Chapter 2. Effect of charge blocking layer for enhancing detectivity in near-infrared organic photodetectors

## 2.1 Introduction

Reducing dark current density is very important issue for enhancing the detectivity of photodetectors. The dark current is originated from injected current from electrode, thermally generated current at PN junction, and leakage current in device. There are many researches on method for reducing dark current density of organic photodetectors such as using charge blocking layer, work function modification.

$$J_{dark} = J_{injection} + J_{generation} + J_{leakage}$$

### 2.1.1 Reviews on method reducing dark current

The methods were reported to reduce dark current of OPDs. Thin cathode was used to tune the work function of ITO electrode. Work function of electrode increased from -4.71 eV to -4.31 eV by depositing MoOx:Al (5nm) on the ITO electrode. Dark current density was reduced due to increasing energetic barrier on injected hole from ITO to HOMO level of acceptor.[8] Likewise, YbF3 as electron transport layer reduced

hole injection current and leakage current.[9] Also, controlling composition of oxygen and nitrogen in silicon oxynitride ($SiO_xX_y$) insulator could tune valance band level and dark current reduced due to the increase of electron injection barrier.[10] But, as shown in **Table 2.1**, research to reduce dark current were conduct mainly in UV-visible OPDs not NIR OPDs. PFN[11,12], ZnO nanowire[13], PFN-OX[14] on the cathode side and PS-TPD-PFCB[15] with HOMO level of -5.6 eV and LUMO level of -2.3 eV on the anode side were used as charge blocking layer. But those were used to block injection carrier and there were no consideration on thermally generated carrier at organic interface.

Not only injected carrier but also thermally generated current at PN junction attribute to dark current in OPDs. To repress both of injection current and generation current, we introduced organic materials which have been used conventionally in organic electronic devices. Many materials have been used for hole injection and transport. Ultimately to reduce the dark current density, material with low HOMO and high LUMO is required.

In our previous research, Near-infrared OPDs using lead phthalocyanine (PbPc) as donor and $C_{60}$ as acceptor were reported. The triclinic phase of PbPc absorbs up to 1050 nm, and the substrate heating and the templating

layer of $C_{60}$ realized NIR light response in bulk heterojunction device. So, EQE of 31.1 % is obtained at -3V and 970 nm, but high dark current density of $3.94 \times 10^{-6}$ A/cm$^2$ is also obtained.[16] So, NPB was used as electron blocking layer to reduce dark current density. Even if not reported, the effect of charge blocking layer was early confirmed in our laboratory by using NPB in this device structure.[17]

In this study, we additionally selected organic materials including NPB between buffer layer of HATCN and PbPc intrinsic layer. The device structure was shown in **Figure 2.1**. 2-TNATA, DNTPD, NPB, TAPC, and CBP were used as charge blocking layer and the dark current density was reduced to 164 nA/cm$^2$ and the enhanced detectivity of $9.7 \times 10^{11}$ cmHz$^{1/2}$/W at 940nm and $1.06 \times 10^{12}$ cm$^2$ Hz/W at 970 nm under reverse bias of -3V were obtained. The detectivity is quite high compared to reported value of $6.7 \times 10^9$ at 810nm and $4.0 \times 10^9$ at 1000nm, -3 V[18], $2.2 \times 10^{10}$ at 900nm, -3V[19].

**Table 2.1**. Literature survey on charge blocking materials to reduce the dark current density of OPDs

| Process | Donor /Acceptor | $J_d$ (A/cm$^2$) | EQE (%) | Detectivity (cm Hz$^{1/2}$/W) | CBL | Ref |
|---|---|---|---|---|---|---|
| S | CuPc: C$_{60}$ | $1.3 \times 10^{-6}$ (-1V) | 51.7 (620nm, -1V) | $4 \times 10^{11}$ (700nm, -1V) | EBL: P6T, BP3T | 34 |
| S | SQ : PCBM | $3.3 \times 10^{-8}$ (-1V) | 15 (700 nm, -1V) | $3.4 \times 10^{12}$ (700nm, -1V) | EBL: PPV | 35 |
| S | SQ:PCBM | $2 \times 10^{-9}$ (-1V) | - | - | EBL:MEH-PPV | 36 |
| S | PBDTTT-C 70-PCBM | $2 \times 10^{-9}$ (-2V) | 30 (680nm, -2V) | ~$10^{13}$ (680nm, -3V) | HBL: PEIE rinsed by QDR | 37 |
| E | DMQA DCV3T | $6.41 \times 10^{-9}$ (-3V) | 55.2 (-3V) | $3.05 \times 10^{12}$ (540nm, -3V) | EBL: TPD15 | 38 |
| S | PTZBTTT-BDT: PC61BM | $4.01 \times 10^{-10}$ (0V) | 18.2 (800nm,0V) | $1.02 \times 10^{13}$ (820nm, -0.5V) | EEL: PFN-OX | 14 |
| S | PDPP3T:PC71BM | $3.1 \times 10^{-10}$ (-2V) | 27 (820nm, -0.5V) | $1.5 \times 10^{12}$ (820nm, -0.5V) | EBL: Poly-TPD | 33 |
| S | P-DTS(FBTTh$_2$)$_2$: PCBM | $1.1 \times 10^{-10}$ (-0.5V) | 67 (700nm, -0.5V) | $9.2 \times 10^{12}$ (700nm, -0.5V) | HBL: C60 | 39 |
| E | DMQA DCV3T | $2.45 \times 10^{-10}$ (-3 V) | 25.8 (540nm, -3V) | $8.95 \times 10^{12}$ (540nm, -3V) | HBL: MoOx:Al WF (0.4eV) | 8 |
| S | PMDPP3T:Pc612BM | $3.1 \times 10^{-7}$ (-3 V) | ~20 (900nm, -3V) | $1 \times 10^{12}$ (950, -3 V) | EBL: m-MTDATA | 40 |
| S | P3HT:PC61BM | $1.02 \times 10^{-7}$ (-3V) | 53.7 (520nm, -1V) | $1.67 \times 10^{12}$ (520nm, -1V) | EBL: NiOx HBL: YbF3 | 41 |
| S | P3HT:PC61BM | $1.13 \times 10^{-7}$ (-3V) | 53.3 (525nm, -1V) | $2.15 \times 10^{12}$ (525nm, -1V) | EBL: NiOx HBL: Yb | 9 |
| S | PCDTBT:PC60BM | $3.1 \times 10^{-10}$ (-2V) | 65 (528nm, -2V) | $3.21 \times 10^{13}$ (566nm, -2V) | HBL: PEIE WF | 42 |
| S | PBDTT-FTTE:PC70BM | $2.98 \times 10^{-8}$ (-5V) | ~60 (690nm, -5V) | $3.31 \times 10^{12}$ (690nm, -5V) | HBL: ZnO: PSS WF | 43 |
| S | P3HT:PC61BM | $1.9 \times 10^{-8}$ (-0.5V) | - | $9.1 \times 10^{12}$ (550nm, -0.5V) | EBL: PFN (soluble polymer) | 44 |
| E | NPIDDSe:C60 | $1.8 \times 10^{-10}$ (-3V) | 67 (550nm, -3V) | $10^{14}$ (550nm, -3V) | EBL: SiOxNy (x=0.16, y=0.66) | 10 |
| S | PPDT2FBT:ZnO | ~$4 \times 10^{-9}$ (-1V) $5.9 \times 10^{-9}$ (-3V) | 30 (-1V) | $3.04 \times 10^{12}$ (-1V) | ZnO | 45 |

Process: evaporation/ solution

## 2.1.2 Hole transport materials

We selected several materials as charge blocking materials. 2-TNATA[20] and DNTPD[21] have used as hole injection layer due to high HOMO levels for injection of holes from the electrode. NPB was broadly used both in OLEDs and OPVs as hole transport materials.[22] TAPC has very high hole mobility and used as electron blocking layer due to high LUMO level[23] in OLEDs and CBP used as host materials for blue OLEDs[24,25]. The molecular structure of CBL and photoactive materials were shown in **Figure 2.2**. Energy levels of charge blocking materials (CBMs) shown in **Figure 2.3** were measured even though that of CBMs were reported in many papers due to the different value reported in each literature. As shown in absorption spectra of **Figure 2.4b** charge blocking materials have no absorption in near-infrared region. There was no contribution by absorption on the enhancement of EQE.
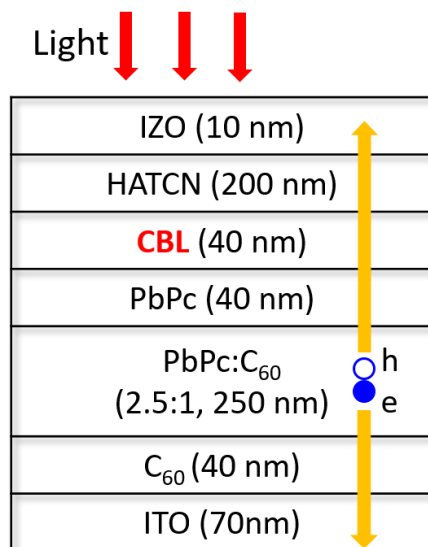
**Figure 2.1** Inverted device structure of PbPc based NIR OPD. The Light is incident from top electrode of IZO and electrons were extracted and collected to ITO bottom electrode.
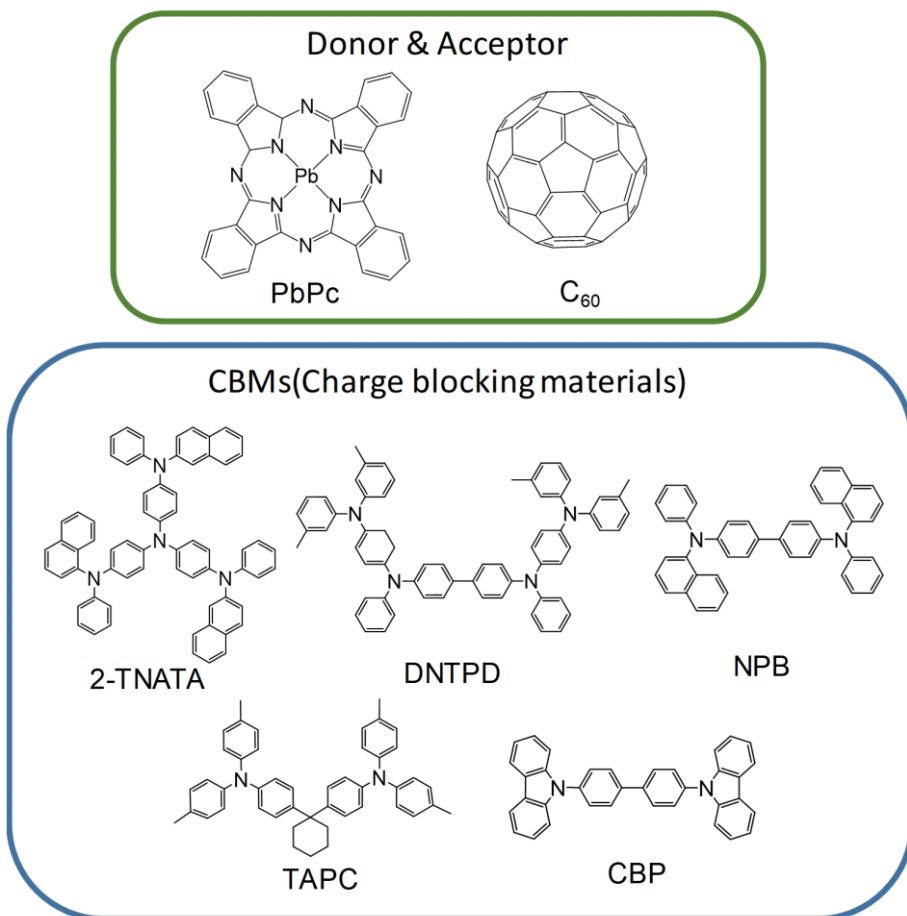
**Figure 2.2** Molecular structures of donor, acceptor, and charge blocking

materials including 2-TNATA, DNTPD, NPB, TAPC, and CBP
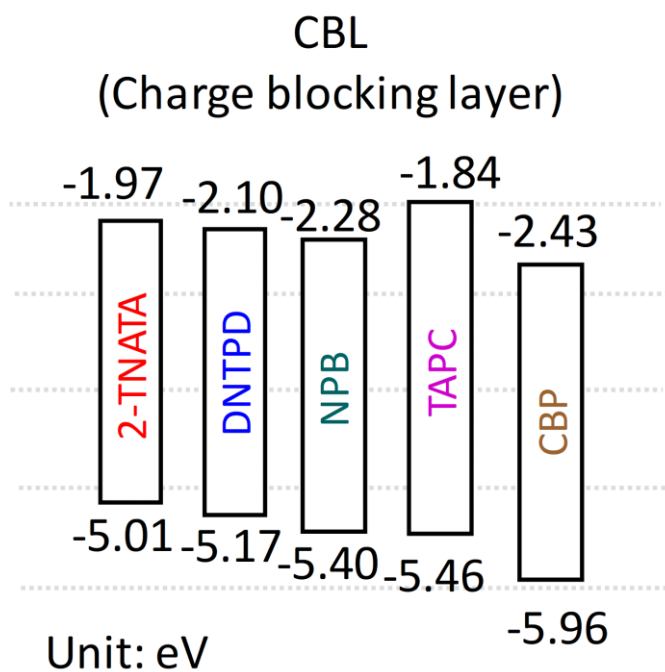
**Figure 2.3** Schematic energy diagram of charge blocking materials, 2-TNATA, DNPTD, NPB, TAPC, and CBP

## 2.2 Experimental methods

### 2.2.1 Materials

Lead phthalocyanine (PbPc; purity of 95%) was purchased from TCI chemicals and sublimated once in our laboratory. Fullerene-C60, 4,4',4''-Tris[2-naphthyl(phenyl)amino]triphenylamine (2-TNATA; 99.9%, EM index, Korea ), N,N'-bis[4-[bis(3-methylphenyl)amino]phenyl]-N,N'-diphenyl- (DNTPD; 99.9%, Nichem, Taiwan), N,N'-di(1-naphthyl)-N,N'-diphenyl-(1,1'-bisphenyl)-4,4'-diamine (NPB; 99%, Nichem, Taiwan), 4,4'-cyclohexylidenebis [N,N-bis(4-methylphenyl)benzenamine] (TAPC, shine materials, Taiwan), 4,4'-bis(N-carbazolyl)-1,1'-biphenyl (CBP; 99%, Nichem, Taiwan), and 1,4,5,8,9,11-Hexaazatriphenylenehexacarbonitrile (HATCN; 99%, Nichem, Taiwan ) were used as received without further purification.

### Absorption spectra

Ultraviolet-visible (UV-vis) absorption spectra were recorded using a Varian Cary 500 UV-vis spectrophotometer. Methylene chloride (MC) was used as the solvent and the concentration is $10^{-5}$ M.

### Measurement of energy level

Energy levels of charge blocking materials (CBMs) including 2-TNATA, DNTPD, NPB, TAPC, and CBP were measured via method of cyclic

voltammetry. The NPB is set as reference material with HOMO level of -5.4 eV and HOMO levels of other materials are relatively determined to that of NPB. The solutions of $10^{-3}$M were used and tetrabutylammonium hexfluorophosphate (TBAPF6) of 0.1M was added as electrolyte and
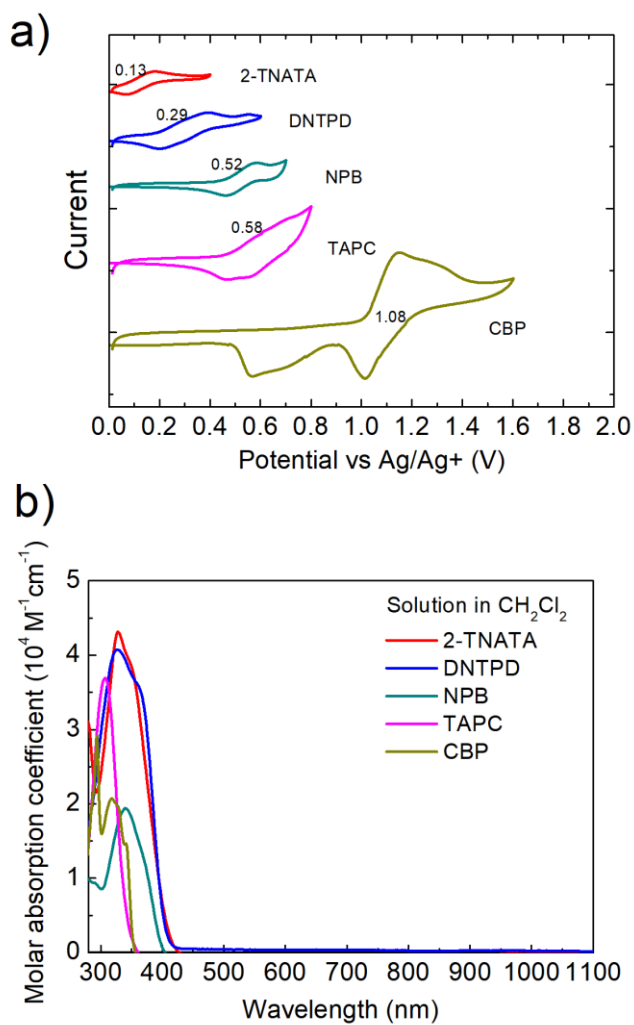
**Figure 2.4** a) Current-Potential (vs Ag/Ag+) curve, b) absorption spectra
of charge blocking materials

## 2.2.2 Fabrication of devices

The structure of inverted OPD of ITO (70 nm)/ $C_{60}$ (40 nm)/ PbPc:$C_{60}$ (ratio of 2.5:1, 250 nm)/ PbPc (40 nm)/ CBL (40nm)/ HATCN (200 nm)/ IZO (10 nm) are shown in **Figure 2.1**.

The ITO coated glass substrates were cleaned with detergent solution, acetone, and isopropyl alcohol to remove particles and organic impure materials. A $C_{60}$ layer, mixed layer of PbPc and $C_{60}$, PbPc layer, CBL layer, and HATCN layer were deposited at a rate of 0.5 Å/s, 0.2 Å/s, 1.0 Å/s, 0.5 Å/s, and 0.2 Å/s respectively. The substrate was heated to 180 °C during deposing mixed layer to form triclinic phase of PbPc for NIR absorption.[26] Except for mixed layer the temperature of the substrate was under 20 °C during depositing all layers. HATCN served as a buffer to protect the organic layers from sputtering damage during the formation of the IZO top electrode via sputtering. All of the organic layers were deposited at a base pressure under $1 \times 10^{-7}$ Torr.

The substrate was transferred through the glove box and metal carrier to another chamber to form IZO top electrode on the HATCN layer using a sputtering process. Sputtering took place under gas flow rates of 30 sccm for Ar and 0.6 sccm for $O_2$, and working pressure of 1.9 mTorr. After sputtering process, the devices were encapsulated in a $N_2$ atmosphere.

### 2.2.3 Characteristics of devices

The current density-voltage (J-V) characteristics were measured by using a Keithley 237 source measurement unit. The EQE spectra under the short circuit and the reverse biased voltage were measured using a 1000W Xe lamp (Oriel) combined with a calibrated monochromator (Acton Research). The intensity of monochromatic light was calibrated with the aid of a silicon photodiode (Newport).

## 2.3 Result and discussion

**A relationship between energy level of CBL and dark current density**

CBLs were inserted between PbPc and HATCN layer. When the reverse bias is applied to device, electron and hole are injected from IZO and ITO respectively. In case of the hole, the energy barrier between ITO and the layer of $C_{60}$ is 1.7 eV. On the other hand, electron injection barrier between the layer of HATCN and the layer of PbPc is 0.8 eV and is lower than the injection barrier for hole. So, using electron blocking layer is more effective on change of current and voltage characteristics. Schematic diagram of inverted near-infrared OPDs with CBL is shown in **Figure 2.5**.

The current density and voltage characteristics of devices with or without CBLs under dark and illumination of 940nm light source conditions are shown in **Figure 2.6a**. The device without CBL had dark current as high as 3473 $nA/cm^2$ at -3V. But the dark current density was reduced to 1192 $nA/cm^2$ when 2-TNATA was inserted between the layer of HATCN and the layer of the PbPc. It means that injected electrons from IZO electrode were blocked by high LUMO of 2-TNATA between the layer of HATCN and the layer of the PbPc.
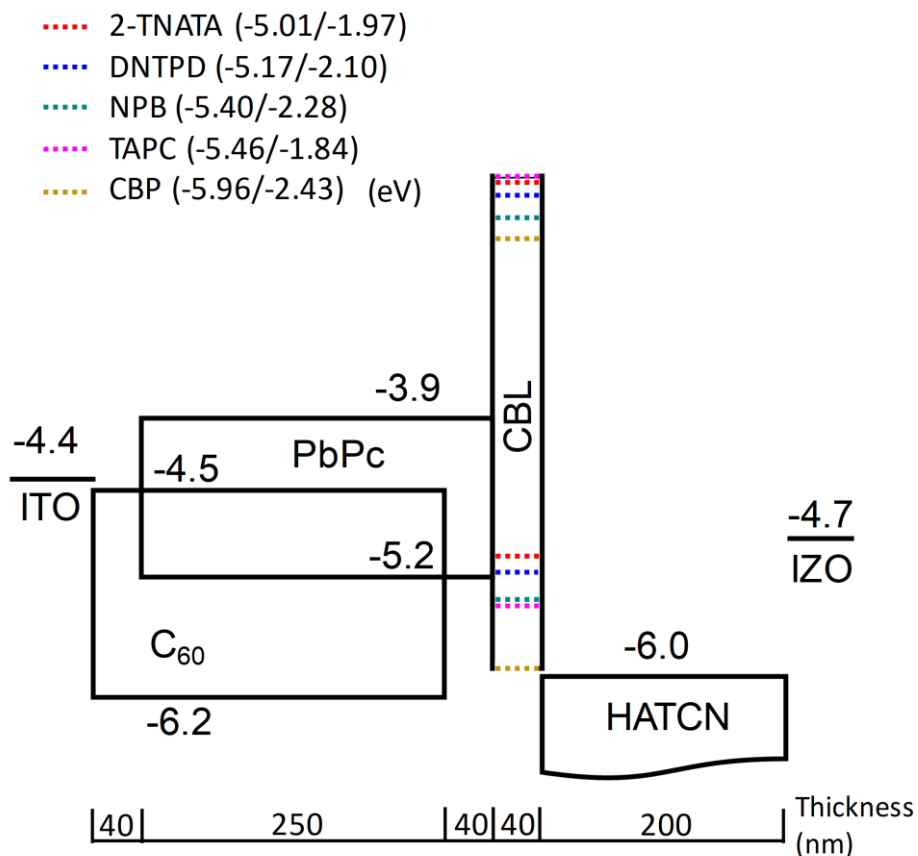
**Figure 2.5** Schematic diagram of inverted near-infrared OPDs with charge blocking layers. There is energetic barrier in device with CBL layer due to high LUMO level and deep HOMO level of chare blocking layers.

However, the dark current density further decreased to 304 nA/cm$^2$, 217 nA/cm$^2$, and 164 nA/cm$^2$ when using NPB, TAPC, and CBP respectively even though in case of NPB and CBP HOMO is lower than that of 2-TNATA. It means there are not only injection barrier on electron but also extraction barrier on thermally generated charge at interface PN junction or excited to trap state[27]. As seen in **Figure 2.7,** thermally generated charges were accumulated at the interface between PbPc and NPB and not extracted due to lower HOMO level of NPB of -5.4 eV than PbPc of -5.2 eV. The same results were exhibited in case of TAPC and CBP. When DNTPD was used, the dark current density also decreased even though LUMO of DNTPD is lower than that of 2-TNATA and HOMO level is higher than that of PbPc. It is not yet interpreted clearly, but HOMO level offset between DNTPD and PbPc is as small as 0.03 eV, so energy level alignment could be different with expectation.

From J-V characteristics, we could investigate the effect of energetic barrier on the dark current density by changing HOMO of CBL. **Figure 2.6b** shows the change of dark current density as a function of the HOMO level of CBL. It is not quantitative interpretation but, it can be helpful to understand the origin of dark current.
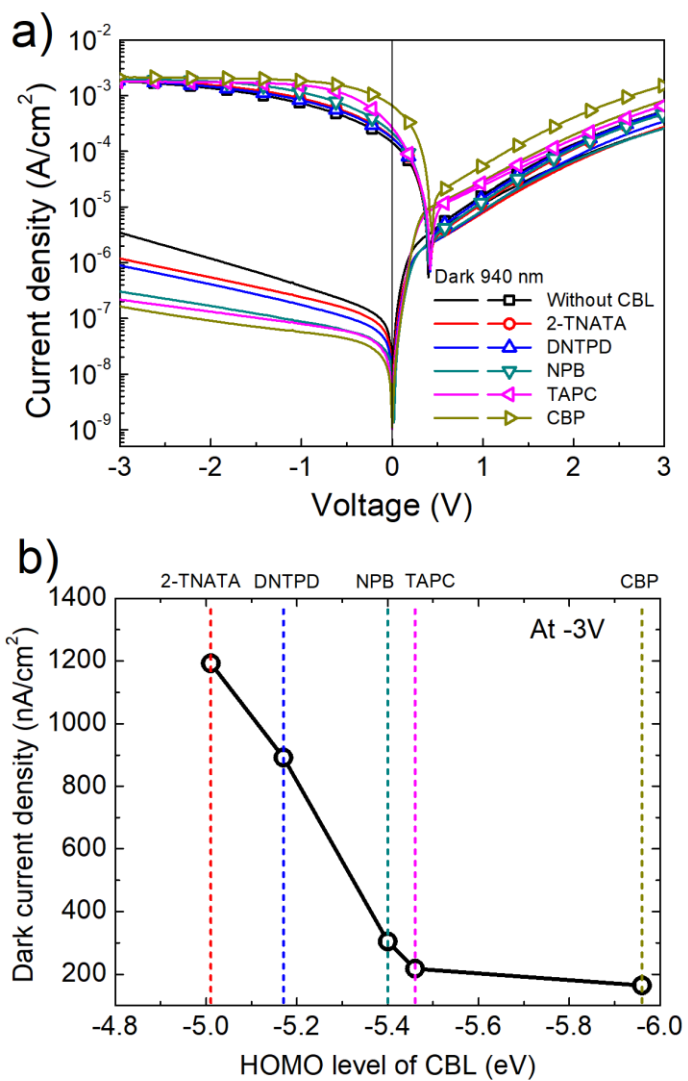
**Figure 2.6** a) Device characteristics of current density-voltage characteristics under dark and illumination of 940 nm conditions, b) change of dark current density as function of HOMO level of CBLs
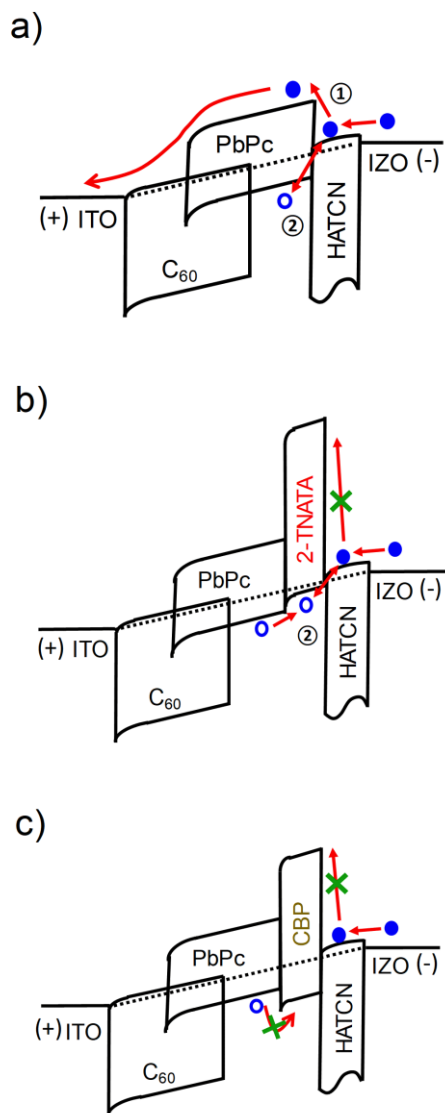
**Figure 2.7** Schematic energy diagram under dark condition. a) without CBL, b) with 2-TNATA blocking electron injected from IZO, c) with CBP blocking both of electron injected from IZO and blocking hole extracted to IZO

EQE spectra were measured at various bias. **Figure 2.8d** shows the increase of EQE with increasing reverse bias but, there was no large increase above -1V and it seems that photo-induced charges almost were extracted even low voltage like -1V. Interestingly, there are differences of EQE depending on CBL, especially at zero bias. The device without CBL exhibited EQE of 6 % at 0V, however, the device with CBP exhibited the EQE of 15 %. Because CBMs have no absorption in region of NIR wavelength it is thought the charge transport is enhanced between CBLs and HATCN due to charge generation. HATCN has been used for charge injection generally in OLED[28,29] and extraction in organic and perovskite solar cell.[30,31,32] In our study, 200nm HATCN was used for protecting organic materials from damage of sputtering forming IZO and extracting holes. Although HATCN has been used as p-dopant, there are different charge extraction efficiency depending on hole transport materials, in this case CBLs. CBP has low HOMO levels of -5.96 eV, which facilitate to generate charge due to energy difference is small around 0.1eV. It was assumed the loss of transport from PbPc to CBL is negligible due to a number of photo-induced charges.

As shown in **Table 2.3**, open circuit voltage in each device was similar but, the short circuit current density of CBP are 4-fold increased to 1.6 mA/cm$^2$. Parallel resistances ($R_s$) were fitted with diode equation and it consistent with the change of dark current density. Reduced dark current

density and increased EQE results in enhancing the detectivity. The calculated detectivity and responsivity spectra were shown in **Figure 2.9**. As expected, the detectivity of the device with CBP is noticeably higher than other devices at zero bias due to high EQE of although the dark current densities are similar. The high detectivity was obtained $7.16 \times 10^{12} \, cm^2 \, Hz/W$ at zero bias and $1.06 \times 10^{12} \, cm^2 \, Hz/W$ at -3V.

We could plot the dark current density, EQE, and the detectivity as the function of the HOMO level of CBLs shown in **Figure 2.10**. At -3V, the EQE is similar but the dark current density is dramatically reduced until HOMO of -5.46 eV. The detectivity increased as the HOMO level is deeper and when the reverse bias is applied, reducing the dark current density more effective on enhancing the detectivity.
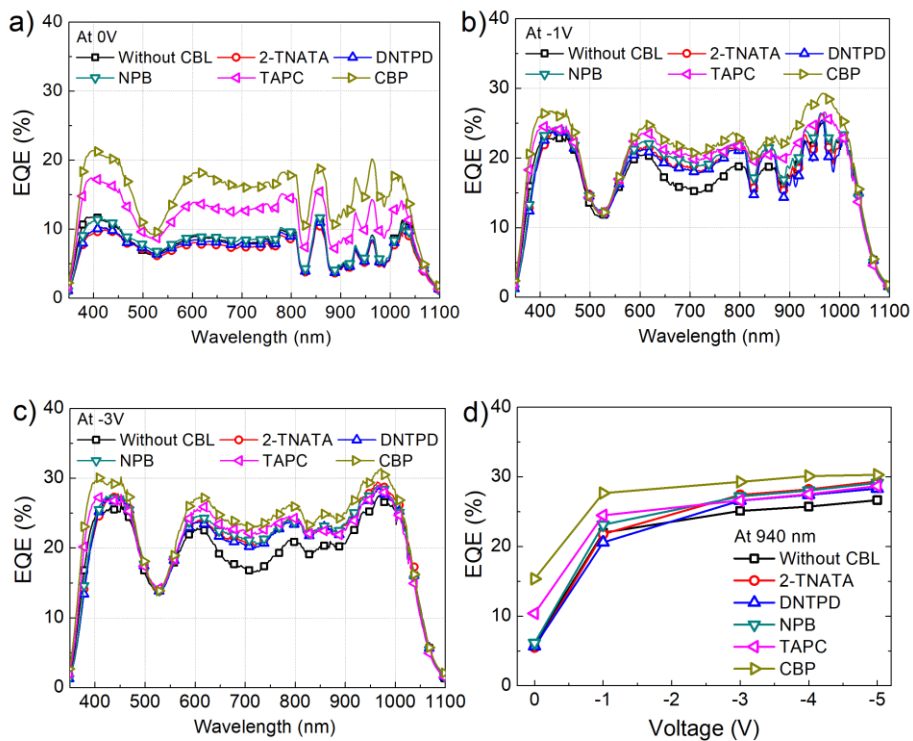
**Figure 2.8** EQE spectra were measured at a) 0V, b) -1V, and c) -3V respectively. d) EQE-voltage relation shows EQE were saturated above -3V with increase of reverse bias.
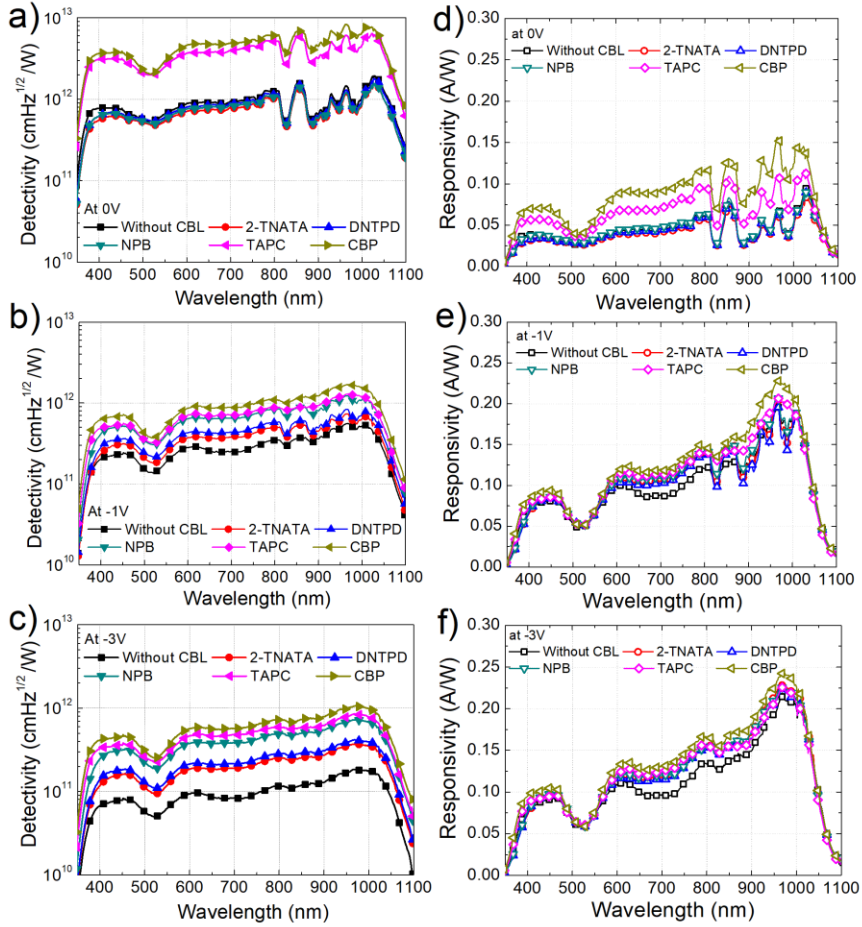
**Figure 2.9** The detectivity and responsivity were calculated with dark current density and EQE The device with CBP represented highest detectivity at all bias.
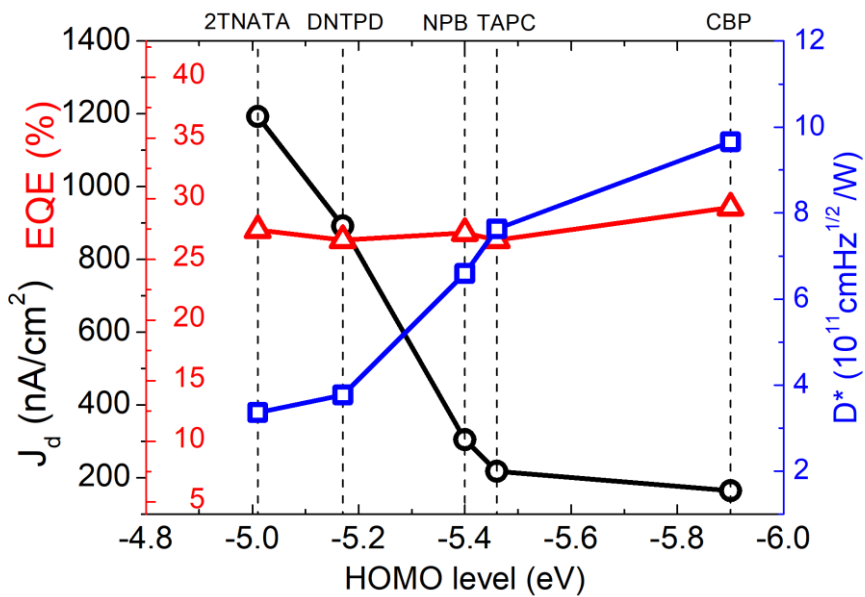
**Figure 2.10** The dark current density, EQE, and the detectivity at -3V and 940 nm were plotted as function of the HOMO level of CBLs.

**Table 2.2** numerical parameters of inverted device structure of PbPc based NIR OPD. The dark current density ($J_d$), EQE, specific detectivity (D*), and responsivity (R) of OPDs depending on charge blocking layer are listed. The detectivity and responsivity were calculated from EQE and dark current density at -3V, 940 nm.

| OPDs | CBL | $J_d$ (nA/cm$^2$) | | | EQE (%) | | | D* (cm Hz$^{1/2}$/W) | R (A/W) |
|---|---|---|---|---|---|---|---|---|---|
| | | 0V | -1V | -3V | 0V | -1V | -3V | | |
| 1 | Without CBL | 7.4 | 381 | 3473 | 6.02 | 22.0 | 25.1 | $1.6 \times 10^{11}$ | 0.190 |
| 2 | 2-TNATA | 9.3 | 241 | 1192 | 5.47 | 21.8 | 27.4 | $3.4 \times 10^{11}$ | 0.207 |
| 3 | DNTPD | 8.0 | 174 | 891 | 5.65 | 20.6 | 26.6 | $3.8 \times 10^{11}$ | 0.201 |
| 4 | NPB | 11 | 88 | 304 | 6.12 | 23.1 | 27.2 | $6.6 \times 10^{11}$ | 0.206 |
| 5 | TAPC | 1.0 | 79 | 217 | 10.4 | 24.5 | 26.6 | $7.6 \times 10^{11}$ | 0.201 |
| 6 | CBP | 1.1 | 57 | 164 | 15.3 | 27.7 | 29.3 | $9.7 \times 10^{11}$ | 0.222 |

**Table 2.3** Energy levels, $V_{OC}$, short circuit current density ($J_{sc}$), and parallel resistance ($R_P$) were listed. The photocurrent density was measured under 1 sun illumination. The parallel resistances were extracted from J-V curves by using diode equation around zero bias.

| OPDs | CBL | HOMO (eV) | LUMO (eV) | $V_{OC}$ (V) | $J_{sc}$ (mA/cm$^2$) | $R_P$ ($\Omega$ cm$^2$) |
|------|-----|-----------|-----------|--------------|----------------------|--------------------------|
| 1 | Without CBLs | - 5.2 | -3.9 | 0.40 | 0.44 | $2.66 \times 10^6$ |
| 2 | 2-TNATA | -5.01 | -1.97 | 0.42 | 0.49 | $5.52 \times 10^6$ |
| 3 | DNTPD | -5.17 | -2.10 | 0.42 | 0.45 | $8.02 \times 10^6$ |
| 4 | NPB | -5.4 | -2.28 | 0.42 | 0.48 | $1.60 \times 10^7$ |
| 5 | TAPC | -5.46 | -1.84 | 0.42 | 0.63 | $1.80 \times 10^7$ |
| 6 | CBP | -5.96 | -2.43 | 0.42 | 1.6 | $2.47 \times 10^7$ |

## 2.4 Conclusion

We focused on the dark current density bias for enhancing the detectivity of NIR OPDs under reverse. The dark current density consists of injection carrier from the electrode and thermally generated charge at the interface of donor and acceptor and trap state in organic layer. We introduced charge blocking layer with various energy level to reduce the dark current density. As a result, the dark current density reduced as HOMO level of CBL became deeper. In this experiment, it was found high LUMO blocked injected electron from the anode and low HOMO also suppressed extracted hole to the anode. The low dark current density of 164 nA/cm$^2$ was obtained. Also, the enhanced EQE of 15 % was obtained in the device with CBP at 0V due to efficient hole transport due to charge generation between CBP and HATCN.

Conclusively, reduced dark current density and increased EQE resulted in enhancing detectivity and it reached 1.06 $\times 10^{12}$ cm$^2$ Hz/W at -3V and 970nm. It is the very high value of the detectivity among the NIR OPDs working around the reverse bias of -3V.

# Chapter 3. Figure of merits in near-infrared organic photodetectors

## 3.1 Introduction

Other important figure of merits in OPDs includes linear dynamic range, cut off frequency, and response time. We achieved low dark current density and high detectivity using charge blocking layers such as CBP and TAPC. Insertion of charge blocking layer influenced on dynamic characteristics of the device although it is not related to efficiency like responsivity. In this chapter, we measured and compared the devices with the different charge blocking layer.

## 3.2 Experimental methods

**Linear dynamic range (LDR)**

The current density-voltage (J-V) characteristics were measured by using a Keithley 237 source measurement unit. The light source of 940nm illumination was offered by using a 1000W Xe lamp (Oriel) combined with a calibrated monochromator (Acton Research). The

intensity of monochromatic light was calibrated with the aid of a silicon photodiode (Newport) and controlled by neutral density filter.

**Cut off frequency and fall time**

A function generator (32250A 80MHz, Agilent) was used to supply the ac input signal of incident light. An oscilloscope recorded frequency response of the photo-induced signal. The green diode laser (532nm, coherent) was used as light source and connected to the function generator in order to give sinusoidal or square wave on the device. **Figure 3.1** illustrated experimental set up for measuring cut off frequency and response time.
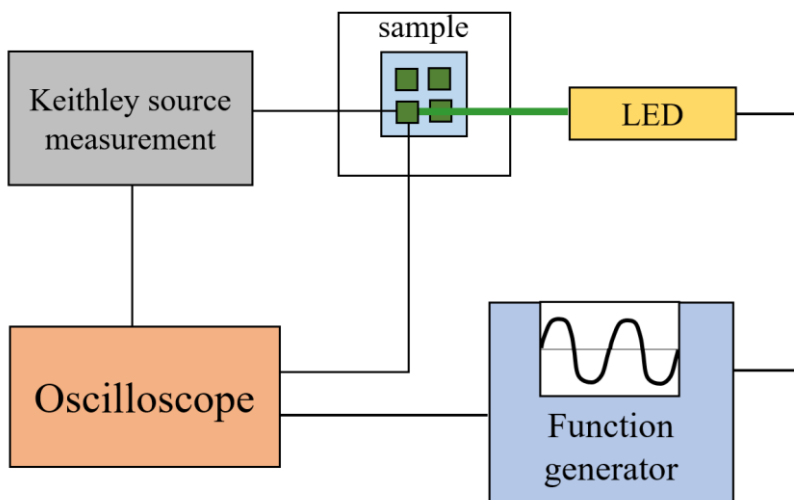
**Figure 3.1** Schematic diagram of experimental set up for measuring cut off frequency and response time of OPDs.

## 3.3 Result and discussion

### 3.3.1 Linear dynamic range (LDR)

**Figure 3.2a, b** shows photocurrent response on light intensity measured at 0V and -3V respectively. There were different tendencies depending on the applied bias to the device. Firstly, all the OPDs measured at zero bias showed linearity in the region of low light intensity but the deviation in region of high light intensity related to the loss of the photocurrent as a result of bimolecular recombination.[33] Among them, the device with CBP represented longer linearity at high light intensity because charge generation efficiency between CBP and HATCN was high. On the other hand, the device measured at -3V exhibited deviation in the region of low light intensity unlike the condition of zero bias. Even though high intensity light was exposed, charge carriers were easily extracted by external force before holes and electrons recombine. The deviation at low intensity is due to the dark current density which is higher than photo-induced current.
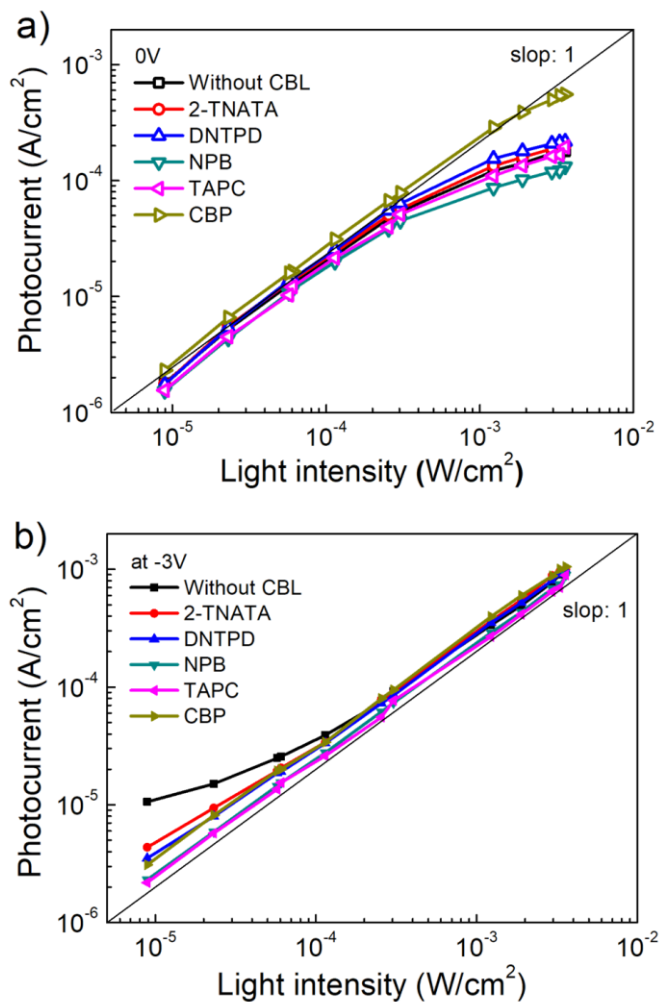
**Figure 3.2** Photocurrent response of the photodetectors with various CBL and without CBL measured at a) 0V and b) -3V. The light source was monochromatic light of 940nm.

### 3.3.2 Fall time ($t_f$)

Fall time is time taken to reach from 90% to 10% of photocurrent after light turned off. Square wave light signal of 0.1Hz was used and the response of photocurrent was shown in **Figure 3.3**.

The devices with CBL have longer decay time than the device without CBL. Charges trapped or accumulated at interface of each organic layer or trapped are extracted to electrode after the light turn off, which caused delayed behavior. In this device, charge blocking layer make band bending at the interface of PbPc and CBL and if it has trap state inside bandgap delayed behaviors can happen. Except for the device without CBL, similar fall times were observed irrespectively on CBL.
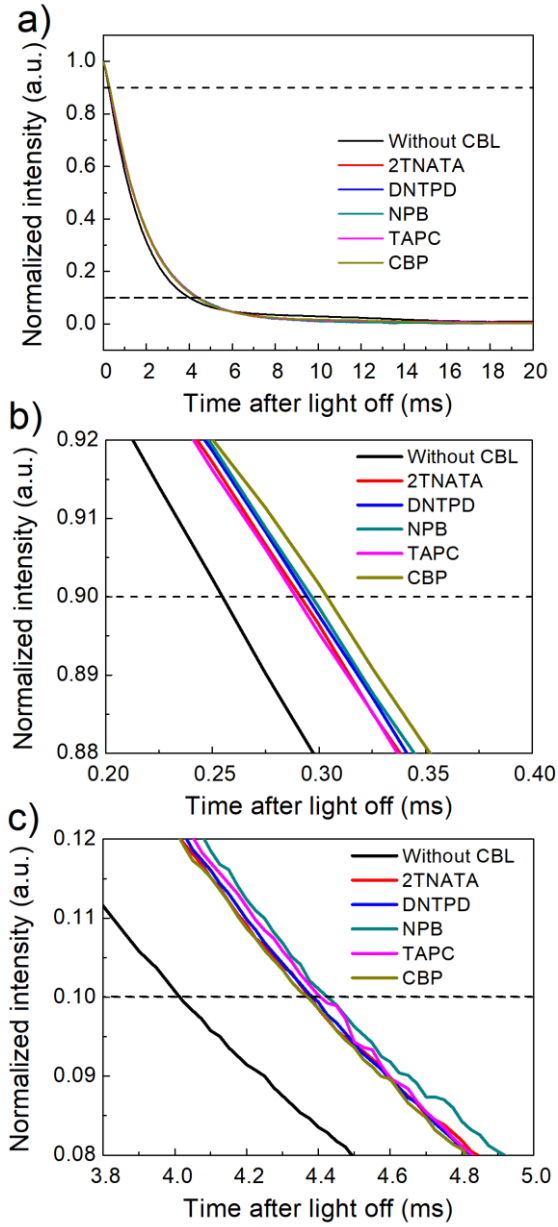
**Figure 3.3** Photocurrent response of the OPDs with various CBL and without CBL. Fall time was increased in the devices with CBLs

### 3.3.3 Cut-off frequency

Frequency response of OPDs were shown in **Figure 3.4**. For the same reason with delayed fall time, the device without CBL has the highest cut-off frequency. However, CBP and 2-TNATA have relatively low response of frequency as 132 and 170 Hz compared to other devices. The reason of low cut-off frequency in the devices with CBP and 2-TNATA is due to low hole mobility of CBP and 2-TNATA as shown in **Figure 3.5**. Under low frequency, there is enough time for holes to be extracted to the electrode. However, as frequency of light increases, the holes could not reach to the electrode before light turns on. And the loss of frequency could be reduced by using materials with high carrier mobility like TAPC.
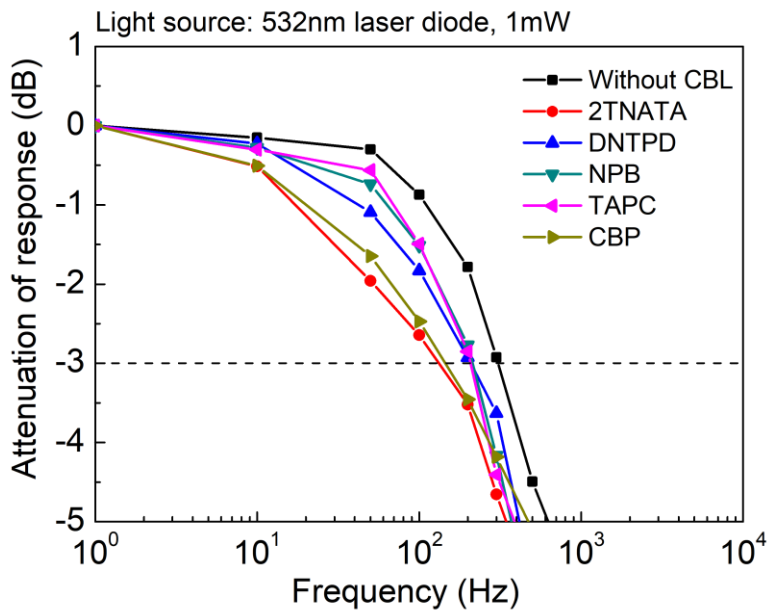
**Figure 3.4** Frequency response of the photodetectors with various CBL and without CBL. The 532nm laser diode was used as light source connected to function generator to make light modulation.

**Table 3.1** Fall time and cut off frequency of OPDs without and with CBL. Fall time was measured when modulated light of 0.1Hz was illuminated. The hole mobility at 0.3V/cm were compared.

| | Device | $t_f$ (ms) | $f_{-3dB}$ (Hz) | Hole mobility ($cm^2/Vs$) |
|---|---|---|---|---|
| 1 | Without CBL | 3.76 | 306 | - |
| 2 | 2-TNATA | 4.09 | 132 | $8.0\times10^{-6}$ |
| 3 | DNTPD | 4.09 | 207 | $1.4\times10^{-5}$ |
| 4 | NPB | 4.13 | 213 | $1.3\times10^{-5}$ |
| 5 | TAPC | 4.12 | 207 | $2.9\times10^{-5}$ |
| 6 | CBP | 4.07 | 170 | $7.4\times10^{-6}$ |

**Hole Mobility of CBMs**

Single carrier device was fabricated to compare hole mobility of CBLs as followed structure.

ITO (150 nm)/ ReO$_3$ (1 nm)/ CBL (100 nm)/ ReO$_3$ (1 nm)/ Al (100 nm).

Mobility is analyzed by space charge limited current (SCLC) method. Current density and mobility are expressed by Mott-gurney theory and Pool-Frenkel model.

$$J_{SCLC} = \frac{9}{8} \varepsilon_0 \varepsilon_r \mu \frac{V^2}{L^3} \tag{3.1}$$

$$\mu = \mu_0 \exp(0.89\beta\sqrt{F}) \tag{3.2}$$

J= the current density

$\varepsilon_0$= vacuum permittivity

$\varepsilon_r$= dielectric constant

$\mu$= mobility

V= voltage

L= thickness of the film.

$\beta$=Pool-Frenkel coefficient

F= electric field

The hole mobilities were shown as a function of electric field in **Figure 3.5b** and that of 0.3V/cm were compared in **Table 3.1**
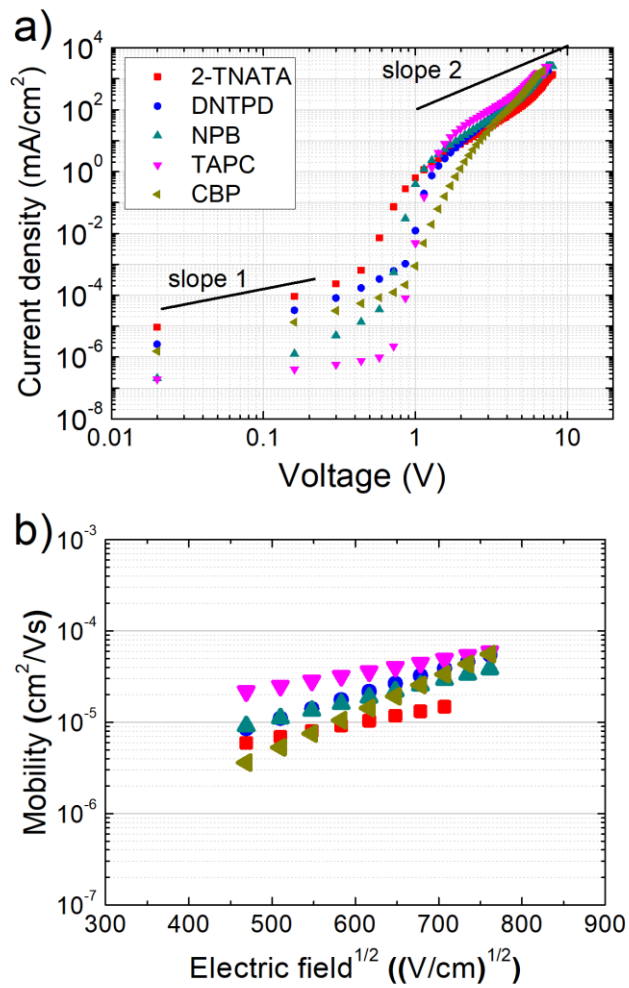
**Figure 3.5** a) Current density-voltage characteristics of single carrier devices. b) The hole mobility of CBLs as function of electric field.

## 3.4 Conclusion

In this chapter, we measured linear dynamic range, fall time, and cut off frequency. Linear dynamic range increased by using CBL due to low dark current density compared to the device without CBL. Also, due to applied reverse bias there is no deviation at high intensity, which is advantage of photoconductive mode photodetectors. But, fall time is longer in all the device with CBL due to the delay of charge extraction originating from charge trapped at charge blocking layer and accumulated at the interface between PbPc and charge blocking layer. Fall time is similar except for the device without CBL. Finally, cut off frequency is quite different between the devices. As the same result with response time, the device without CBL represented highest cut off frequency. On the other hands, inserting the charge blocking layer caused reduction of frequency response. But, the device with TAPC has high response among the devices with CBL. The result means high mobility of charge blocking materials can minimize frequency response loss.

# Chapter 4. Summary and outlook

Organic photodetectors are promising electronic devices following OLEDs. **In chapter 1**, we introduced OPDs with working principles application. And the figure of merits of OPDs were introduced such as detectivity, responsivity, linear dynamic range, response time, and cut off frequency.

**In chapter 2**, we focused on the dark current density of the photodetector related to detectivity meaning sensitivity of the device. To reduce the dark current density, we review on charge blocking layers (CBLs) in OPDs and applied it to NIR OPDs. Charge blocking materials were selected to investigate the origin of the dark current density. The dark current density was reduced by using 4,4'-bis(N-carbazolyl)-1,1'-biphenyl (CBP) as 164 nA/cm$^2$ at -3V. High LUMO of CBP effectively blocked electrons injected from IZO and low HOMO of CBP also blocked hole extracted to IZO. Also, EQE increased because CBP is strong electron donating material and HATCN is strong electron withdrawing material so, hole transporting is favorable.

**In chapter 3,** we continued to study on other figure of merits such as linear dynamic range, response time, and cut off frequency. Linear dynamic range increased due to the reduced dark current density. But,

fall time is longer in the device with CBL which was delayed by trapped charges in bandgap of CBL and accumulated at the interface of organic layer. Finally, cut off frequency also was reduced but, high carrier mobility can minimize the loss of frequency response.

In this thesis, we have focused on enhancing the detectivity of photoconductive mode NIR OPDs and wish this study could propose a criterion for selecting the charge blocking layer when studying characteristics of OPDs.

# Bibliography

[1] G. Yu, J. Wang, J. McElvain, and A. J. Heeger, *Adv. Mater.* **10**, 17 (1988)

[2] D. Baierl, L. Pancheri, M. Schmidt, D. Stoppa, G.-F. D. Betta, G. Scarpa1, and P. Lugli1, *Nat commun.*, **3**, 1175 (2012)

[3] S. Takada, M. Ihamaa, M. Inuiyaa, T. Komatsub, T. Saitob, *SPIE-IS&T*, **6068**, 60680A (2006)

[4] G. Simone, Dario Di Carlo Rasi, X. de Vries, Gaël H. L. Heintges, Stefan C. J. Meskers, René A. J. Janssen, and G. H. Gelinck, *Adv. Mater.* **30**, 1804678 (2018)

[5] P. G. Datskos, N. V. Lavrik, Oak Ridege National Lab.

[6] R. D. Jansen-van Vuuren, A. Armin, A. K. Pandey, P. L. Burn, and P. Meredith, *Adv. Mater.* **28**, 4766 (2016)

[7] H. Jin, A. Armin, M. Hambsch, Q. Lin, P. L. Burn, and P. Meredith, *Phys. Status Solidi A* **212**, 2246 (2015)

[8] D.-S. Lee, K.-H. Lee, Y.-N. Kwon, D.-J. Yun, K.-B. Park, S.-J. Lim, K.-S. Kim, Y. W. Jin, and S. Lee, *Organic Electronics* **24**, 176 (2015)

[9] S. B. Lim, C. H. Ji, I. S. Oh, and S. Y. Oh, *J. Mater. Chem. C.* **4**, 4920 (2016)

[10] S. Heo, J. Lee, S. H. Kim, D.-j. Yun, J.-B. Park, K. Kim, N.J. Kim, Y. Kim, D. Lee, K.-S. Kim, and H. J. Kang. *Sic. Rep.* **7**, 1516 (2017)

[11] X. Hu, Y. Dong, F. Huang, X. Gong and Y. Cao. *J. Phys. Chem. C* **117**, 6537 (2013)

[12] L. Li, Y. Huang, J. Peng, Y. C., and X. Peng. *J. Mater. Chem. C.* **2,** 1372 (2014)

[13] T. Yang, K. Sun, X. Liu, W. Wei, T. Yu, X. Gong, D. Wang, and Y. Cao. *J. Phys. Chem. C* **116**, 13650 (2012)

[14] X. Hu, K. Wang, C. Liu, T. Meng, Y. Dong, S. Liu, F. Huang, X. Gong, and Y. Cao. *J. Mater. Chem. C.* **2,** 9592 (2014)

[15] X. Gong, M. Tong, Y. Xia, W. Cai, J. S. Moon, Y. Cao, G. Yu, C.-L. Shieh, B. Nilsson, and A. J. Heeger, *SCIENCE* **325,** 1665 (2009)

[16] M.-S. Choi, S. Chae, H. J. Kim, J.-J. Kim, *ACS Appl. Mater. Interfaces* **10**, 25614 (2018)

[17] M.-S. Choi. Controlling crystallinity of organic thin films to improve optical and electrical properties in organic optoelectronic devices. Ph. D thesis (2018)

[18] E.-C. Chena, S.-R. Tseng, Y.-C. Chao, H.-F. Meng, C.-F. Wangc, W.-C. Chenc, C.-S. Hsud, and S.-F. Horng, *Synthetic Metals* **161**, 1618 (2011)

[19] S. M. Menke, R. Pandey, and R. J. Holmes. *Appl. Phys. Lett.* **101**, 223301 (2012)

[20] F. X. Zang, T. C. Sum, A. C. H. Huan, T. L. Li, W. L. Li, and F. Zhu. *Appl. Phys. Lett.* **93**, 023309 (2008)

[21] B. D. Chin, *J. Phys. D: Appl. Phys.* **41** 215104 (2008)

[22] G. W. Kim, R. Lampande, D. C. Choe, H. W. Bae, and J. H. Kwon, *Thin Solid Films* **589**, 105 (2015)

[23] J.-H. Lee, S. Lee, J.-B. Kim, J.H. Jang and J.-J. Kim. *J. Mater. Chem.* **22**, 15262 (2012)

[24] D. F. O'Brien, M. A. Baldo, M. E. Thompson, and S. R. Forrest. *Appl. Phys. Lett.* **74**, 442 (1999)

[25] J.-W. Kang, S.-H. Lee, H.-D. Park, W.-I. Jeong, K.-M. Yoo, Y.-S. Park, and J.-J. Kim. *Appl. Phys. Lett.* **90,** 223508 (2007)

[26] M.-S. Choi, S. Chae, H. J. Kim, and J.-J. Kim, *ACS Appl. Mater. Interfaces*, **10**, 25614 (2018)

[27] A. H. Fallahpour, S. Kienitz, and P. Lugli, *IEEE TRANSACTIONS ON ELECTRON DEVICES* **64**, 6, (2017)

[28] J.-H. Lee, S. Lee, J.-B. Kim, J. Jang and J.-J. Kim, *J. Mater. Chem.* **22**, 15262 (2012)

[29] S. M. Park, Y. H. Kim, Y. Yi, H.-Y. Oh, and J. W. Kim, *Appl. Phys. Lett.* **97**, 063308 (2010)

[30] M.-S. Choi, S. Lee, H. J. Kim, J.-J. Kim, *Organic Electronics* **61**, 164 (2018)

[31] Y. Ma, Y.-H. Chung, L. Zheng, D. Zhang, X. Yu, L. Xiao, Z. Chen, S. Wang, B. Qu, Q. Gong, and D. Zou, *Appl. Mater. Interfaces* **7**, 6406 (2015)

[32] Q.-K. Wang, R.-B. Wang, P.-F. Shen, C. Li, Y.-Q. Li, L.-J. Liu, S. Duhm, and J.-X. Tang, *Adv. Mater. Interfaces* **2**, 1400528 (2015)

[33] X. Zhou, D. Yang, and D. Ma, *Adv. Optical Mater.* **3**, 1570 (2015)

[34] Y. Higashi, K.-S. Kim, H.-G. Jeon, and M. Ichikawa, *J. Appl. Phys.* **180**, 034502 (2010)

[35] M. Binda, A. Iacchetti, D. Natali, L. Beverina, M. Sassi, and M. Sampietro, *Appl. Phys. Lett.* **98**, 073303 (2011)

[36] A. Iacchetti, M. Binda, D. Natali, M. Giussani, L. Beverina, C. Fiorini, R. Peloso, and M. Sampietro, *IEEE Transactions on nuclear science* **59**, 1862 (2012)

[37] E. Saracco, B. Bouthinon, J.-M. Verilhac, C. Celle, N. Chevalier, D. Mariolle, O. Dhez, and J.-P. Simonato, *Adv. Mater.* **25**, 6534 (2013)

[38] D.-S. Leem, K.-H. Lee, K.-B. Park, S.-J. Lim, K.-S. Kim, Y. W. Jin, and S. Lee, *Appl. Phys. Lett.* **103**, 043305 (2013)

[39] I. K. Kim, B. N. Pal, M. Ullah, P. L. Burn, S.-C. Lo, P. Meredith, and E. B. Namdas, *Adv. Optical Mater.* **3**, 50 (2015)

[40] S. Xiong, J. Tong, L. Mao, Z. Li, F. Qin, F. Jiang, W. Meng, T. Liu, W. Li, and Y. Zhou, *J. Mater. Chem. C* **4**, 1414 (2016)

[41] S. B. Lim, C. H. Ji, K. T. Kim, and S. Y. Oh, *Journal of the Korean Physical Society* **69**, 3, (2016)

[42] M. Kielar, O. Dhez, G. Pecastaings, A. Curutchet, and L. Hirsch, *Sci. Rep.* **6**, 39201 (2016)

[43] S. Yoon, J. Cho, K. M. Sim, J. Ha, and D. S. Chung, *Appl. Phys. Lett.* **110**, 083301 (2017)

[44] T. Wang, Y. Hu, Z. Deng, Y. Wang, L. Lv, L. Zhu, Z. Lou, Y. Hou, and F. Teng, *RSC Adv.* **7**, 1743 (2017)

[45] S. Yoon, C. W. Koh, H. Y. Woo, and D. S. Chung, *Adv. Optical Mater.* **6**, 1701085 (2018)

# 초  록

유기발광 다이오드를 따라 유기물 광 검출기 또한 많은 연구가 진행되고 있다. 유기물을 사용함으로서 가질 수 있는 낮은 공정 비용, 다양한 기판 선택성, 파장 선택성 등의 장점이 유기물 반도체에 대한 연구의 원동력이 되고 있다.

유기물 광 검출기는 물질의 특정 파장 영역에서 흡수에 따라 다양하게 응용이 가능하다. 근 적외선 광 검출기는 방범용 카메라, 원격 조종, 적외선 카메라 등에 활용될 수 있으며 특히 유기물을 이용하면 인공 망막에도 활용될 수 있는 잠재력이 있다. 하지만 근적외선 유기물 광 검출기는 작은 밴드갭을 가져, 암전류에 의한 노이즈가 크게 나타난다는 문제가 있다. 이는 외부 전압이 가해지는 광전도 방식의 광 검출기에서 특히 암전류가 크게 증가하는 문제가 나타난다. 이는 광 검출기의 검출도를 낮추는 요소가 되고 검출도 향상을 위해서는 암 전류 감소가 요구된다. 암 전류는 전극으로부터 주입되는 전하와 전자 주개와 전자 받개의 계면에서 열적으로 형성되는 전하로 이루어져있다. 따라서

이런 전하의 이동을 막음으로 암 전류를 감소시켜켜 광 검출기의 검출도를 향상시킬 수 있다.

이미지 센서로 구동하기위해 트랜지스터와 결합을 위한 역 구조의 광 검출기가 요구되며, 역 구조의 광 검출기는 상부 투명 전극의 형성으로 유발되는 손상으로 인한 큰 암 전류 밀도를 나타낸다. 따라서 전하 차단 층으로 분자의 에너지 레벨과 정공 이동도가 다양한 물질을 선정하여 전극과 전자 주개 층 사이에 삽입하여 소자를 제작하였다. 그 결과, 4,4'- bis(N-carbazolyl)-1,1'-biphenyl (CBP)를 전하 차단 층으로 사용하였을 때 −3V 에서 164 nA/cm$^2$ 으로 낮은 암전류가 얻어졌으며, 외부 광전 변환효율이 25.1%에서 29.3%로 증가함으로 9.7×10$^{11}$ cm Hz$^{1/2}$/W 의 높은 검출도가 얻어졌다.

이는 전하 차단 층의 높은 LUMO 준위로 전극에서 주입되는 전하에 대한 큰 에너지 장벽과 낮은 HOMO 준위에 의해 전극으로 추출되는 전하의 이동을 막은 것의 결과로 나타났다. 전하 차단층의 HOMO 준위에 따라 암전류가 변화하는 경향을 보였는데, 이는 LUMO 준위가 전극에서 주입되는 전자를

막을 정도로 충분히 높으면 HOMO 준위에 의해 암전류가 감소하는 것을 의미한다.

더 나아가 선형 구동 범위, 차단주파수, 응답 시간 등의 중요한 성능 지수 등을 측정하여 비교하였다. 입사되는 빛의 강도에 따라 광 전류가 선형적으로 변화하는 구간은 암전류가 낮은 소자에서 더 크게 나타났다. 하지만 전하 차단 층을 사용하면 응답 시간이 증가하는 결과가 나타났는데, 이는 두께 증가와 계면에 쌓인 전하가 전극으로 추출이 지연되는 현상에 의한 것으로 여겨진다. 마찬가지로 차단 주파수도 전하 차단 층에 의해 감소하였지만, 전하 이동도가 높은 물질을 사용했을 때는 상대적으로 적은 감소를 보였다.


이 연구를 통해 유기물 광 검출기의 특성에 미치는 전하 차단 층 효과를 알 수 있으며 앞으로 물질 연구 및 소자 구조 개발에 도움이 될 수 있길 바란다.